PHYSICAL REVIEW A **83**, 042517 (2011)

Faddeev random-phase approximation for molecules

Matthias Degroote,[1,*] Dimitri Van Neck,[1] and Carlo Barbieri[2]
[1]*Center for Molecular Modeling, Technologiepark 903, B-9052 Zwijnaarde, Belgium*
[2]*Department of Physics, Faculty of Engineering and Physical Sciences, University of Surrey, Guildford GU2 7XH, United Kingdom*
(Received 1 October 2010; published 27 April 2011)

The Faddeev random-phase approximation is a Green's function technique that makes use of Faddeev equations to couple the motion of a single electron to the two-particle–one-hole and two-hole–one-particle excitations. This method goes beyond the frequently used third-order algebraic diagrammatic construction method: all diagrams involving the exchange of phonons in the particle-hole and particle-particle channel are retained, but the phonons are now described at the level of the random-phase approximation, which includes ground-state correlations, rather than at the Tamm-Dancoff approximation level, where ground-state correlations are excluded. Previously applied to atoms, this paper presents results for small molecules at equilibrium geometry.

DOI: 10.1103/PhysRevA.83.042517 PACS number(s): 31.10.+z, 31.15.A−, 31.15.vn

I. INTRODUCTION

The study of electronic systems by means of first-principles calculations has taken a high rise thanks to modern computer technology [1–5]. The Green's function formalism [6–8] is one of these *ab initio* methods that has been successfully applied in quantum chemistry [9–12]. The correlations in a many-body system are described in terms of an electron self-energy, which acts as an energy-dependent potential describing the motion of a single electron in the many-electron system. The accuracy of the (in principle, exact) Green's function formalism is now governed by the approximation chosen for the electron self-energy.

A particular third-order approximation scheme to the self-energy can be obtained using the algebraic diagrammatic construction [ADC(3)] method as developed by Schirmer and co-workers [13]. This method has proven to be very successful in predicting one-electron properties in molecules [14] as measured, e.g., in electron momentum spectroscopy. Although the ADC(3) equations were derived in a purely algebraic manner, they can be shown to be equivalent to resumming all particle-hole (ph) and particle-particle (pp) interactions between two-particle–one-hole (2p1h) and two-hole–one-particle (2h1p) states up to the Tamm-Dancoff approximation (TDA) [7] level. This is diagrammatically equivalent to considering phonons (defined here as excitations in the ph and pp channels) at the TDA level, and then allowing the exchange of these phonons in all possible ways between the tree propagators describing the 2p1h or 2h1p states.

The TDA allows no ground-state correlations in the construction of the phonons. An improvement in this respect is the random-phase approximation (RPA) [15]. At least for nuclear systems [15], it is known that the RPA performs better at describing collective behavior. Calculations for the electron gas also show that the RPA leads to a correct prediction of the plasmon pole, whereas the TDA completely fails to describe the plasmon spectrum. It is therefore of interest to formulate an analogous theory to ADC(3) that resums the ph and pp interactions up to the RPA level, i.e., replacing the exchange of TDA phonons by the exchange of their RPA counterparts, with the ultimate purpose of arriving at a self-energy approximation that is valid for both finite and extended systems.

Going beyond the TDA level has proven to be very difficult [16]. The Faddeev random-phase approximation (FRPA) [17] has solved this problem by using the Faddeev technique [18] to include RPA phonons in the self-energy. The FRPA method has been successfully applied to both nuclei [19,20] and atoms [21]. It is the aim of this paper to explore the application of this technique to simple molecular systems.

In the second section of this paper, we give an overview of the working equations for the FRPA method. In Sec. III, we present the numerical results for a set of small molecules. A summary is provided in Sec. IV.

II. THEORY

A. Single-particle Green's function

The single-particle motion in an N-body system is described by the single-particle propagator [7,8] (atomic units are used throughout the paper)

$$G_{\alpha,\beta}(t,t') = -i\left\langle \Psi_0^N \middle| \mathcal{T}[a_\alpha(t)a_\beta^\dagger(t')] \middle| \Psi_0^N \right\rangle, \tag{1}$$

where $\mathcal{T}[\ldots]$ represents the time-ordering operator, Ψ_0^N is the exact ground state, and $a_\alpha(t)$ and $a_\alpha^\dagger(t)$ are the addition and removal operators in the Heisenberg representation for an electron in a single-particle state α. For practical calculations, it is more convenient to use the Lehmann representation of the Green's function

$$\begin{aligned} G_{\alpha,\beta}(E) &= \sum_{m>F} \frac{\left\langle \Psi_0^N \middle| a_\alpha \middle| \Psi_m^{N+1} \right\rangle \left\langle \Psi_m^{N+1} \middle| a_\beta^\dagger \middle| \Psi_0^N \right\rangle}{E - \left(E_m^{N+1} - E_0^N\right) + i\eta} \\ &\quad + \sum_{m<F} \frac{\left\langle \Psi_0^N \middle| a_\alpha^\dagger \middle| \Psi_m^{N-1} \right\rangle \left\langle \Psi_m^{N-1} \middle| a_\beta \middle| \Psi_0^N \right\rangle}{E - \left(E_0^N - E_m^{N-1}\right) - i\eta} \\ &= \sum_{m>F} \frac{f_{\alpha,m} f_{\beta,m}^*}{E - \omega_m + i\eta} + \sum_{m<F} \frac{f_{\alpha,m} f_{\beta,m}^*}{E - \omega_m - i\eta}, \end{aligned} \tag{2}$$

where the $\Psi_m^{N\pm1}$ represent exact eigenstates of the Hamiltonian with energy $E_m^{N\pm1}$. This transition to the energy domain

*matthias.degroote@ugent.be

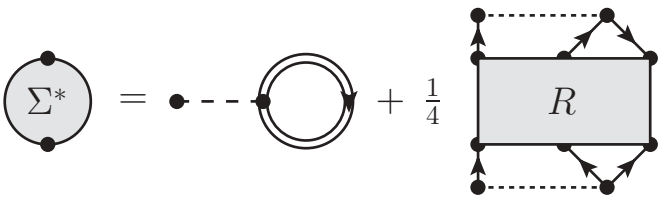

FIG. 1. The Feynman diagram for the irreducible self-energy Σ^* in Eq. (5) within the FRPA. The first diagram represents the HF-type static self-energy.

transforms the Dyson equation from an integral equation into the algebraic relation

$$G_{\alpha,\beta}(E) = G^{(0)}_{\alpha,\beta}(E) + \sum_{\gamma,\delta} G^{(0)}_{\alpha,\gamma}(E)\Sigma^*_{\gamma,\delta}(E)G_{\delta,\beta}(E). \tag{3}$$

In this equation, the exact Green's function G is expressed in terms of the noninteracting $G^{(0)}$ and the irreducible self-energy $\Sigma^*(E)$. Approximation schemes for the single-particle Green's function boil down to finding an appropriate perturbation expansion for the irreducible self-energy.

In our approach, we want to couple the single-particle states with 2p1h and 2h1p states. According to Refs. [22,23], the connection between the irreducible self-energy Σ^* and the six-point response function R can be written as

$$\Sigma^*_{\alpha,\beta}(E) = \Sigma^{\rm HF}_{\alpha,\beta} + \frac{1}{4}\sum_{\lambda,\mu,\nu}\sum_{\epsilon,\theta,\sigma} V_{\alpha\nu,\lambda\mu}R_{\lambda\mu\nu,\epsilon\theta\sigma}(E)V_{\epsilon\theta,\beta\sigma}, \tag{4}$$

where V is the antisymmetrized two-particle interaction and $\Sigma^{\rm HF}$ is the static self-energy as depicted in Fig. 1. We now replace the exact single-energy six-point response function $R(E)$ by an approximate propagator that has indices that are restricted to the 2p1h space ($R^{\rm 2h1p}$) or 2h1p space ($R^{\rm 2h1p}$), and that is exact up to third order:

$$\Sigma^*_{\alpha,\beta}(E) = \Sigma^{\rm HF}_{\alpha,\beta} + \frac{1}{4}\sum_{\lambda,\mu,\nu}\sum_{\epsilon,\theta,\sigma} U_{\alpha\nu,\lambda\mu}R_{\lambda\mu\nu,\epsilon\theta\sigma}(E)U_{\epsilon\theta,\beta\sigma}. \tag{5}$$

The two-particle interaction V in Eq. (4) has been replaced by a second-order expansion

$$U_{\alpha\beta,\gamma\delta} = \sum_{\lambda,\mu}(\mathbb{1}_{\alpha\beta,\lambda\mu} + \Delta U_{\alpha\beta,\lambda\mu})V_{\lambda\mu,\gamma\delta}. \tag{6}$$

This ΔU is needed to guarantee full summation up to third-order perturbation theory and was chosen to be the same as the vertex correction used in the ADC(3) [13].

B. pp or ph RPA interaction

The two-particle propagator [8] is defined by

$$G^{\rm pp}_{\alpha\beta,\gamma\delta}(E) = \sum_m \frac{\langle\Psi^N_0|a_\beta a_\alpha|\Psi^{N+2}_m\rangle\langle\Psi^{N+2}_m|a^\dagger_\gamma a^\dagger_\delta|\Psi^N_0\rangle}{E-\left(E^{N+2}_m - E^N_0\right)+i\eta} - \sum_n \frac{\langle\Psi^N_0|a^\dagger_\gamma a^\dagger_\delta|\Psi^{N-2}_n\rangle\langle\Psi^{N-2}_n|a_\beta a_\alpha|\Psi^N_0\rangle}{E-\left(E^N_0 - E^{N-2}_n\right)-i\eta} \tag{7}$$

$$= \sum_m \frac{\mathcal{X}^{\rm pp}_{\alpha\beta,m}\mathcal{X}^{\rm pp\dagger}_{\gamma\delta,m}}{E-\epsilon^{\rm pp+}_m+i\eta} - \sum_n \frac{\mathcal{Y}^{\rm pp}_{\gamma\delta,n}\mathcal{Y}^{\rm pp\dagger}_{\alpha\beta,n}}{E-\epsilon^{\rm pp-}_n-i\eta}, \tag{8}$$

where the $\mathcal{X}^{\rm pp}$, $\mathcal{Y}^{\rm pp}$, and $\epsilon^{\rm pp}$ are shorthand notations for the overlap amplitudes and energy differences in Eq. (7). A relevant approximation for this object is obtained by solving the RPA equations [15]

$$G^{\rm pp}_{\alpha\beta,\gamma\delta}(E) = G^{\rm pp(0)}_{\alpha\beta,\gamma\delta}(E) - G^{\rm pp(0)}_{\alpha\beta,\delta\gamma}(E) + \frac{1}{2}\sum_{\lambda\mu} G^{\rm pp(0)}_{\alpha\beta,\alpha\beta}(E)V_{\alpha\beta,\lambda\mu}G^{\rm pp}_{\lambda\mu,\gamma\delta}(E) \tag{9}$$

$$= G^{\rm pp(0)}_{\alpha\beta,\gamma\delta}(E) - G^{\rm pp(0)}_{\alpha\beta,\delta\gamma}(E) + G^{\rm pp(0)}_{\alpha\beta,\alpha\beta}(E)\Gamma^{\rm pp}_{\alpha\beta,\gamma\delta}(E)G^{\rm pp(0)}_{\gamma\delta,\gamma\delta}(E), \tag{10}$$

as indicated diagrammatically in Fig. 2(a). Equation (10) defines the effective pp interaction $\Gamma^{\rm pp}$, which includes dynamical screening and will be used later as a building block for the 2p1h and 2h1p interactions. This simple form of the Bethe-Salpeter–type equation for the pp propagator in function of a screened interaction $\Gamma^{\rm pp}$ is possible because the noninteracting pp propagator is diagonal in the Hartree-Fock (HF) basis.

The same procedure can be followed for the particle-hole (ph) polarization propagator [8] [see Fig. 2(b)] defined as

$$\Pi^{\rm ph}_{\alpha\beta,\gamma\delta}(E) = \sum_m \frac{\langle\Psi^N_0|a^\dagger_\beta a_\alpha|\Psi^N_m\rangle\langle\Psi^N_m|a^\dagger_\gamma a_\delta|\Psi^N_0\rangle}{E-\left(E^N_m - E^N_0\right)+i\eta} - \sum_n \frac{\langle\Psi^N_0|a^\dagger_\gamma a_\delta|\Psi^N_n\rangle\langle\Psi^N_n|a^\dagger_\beta a_\alpha|\Psi^N_0\rangle}{E-\left(E^N_0 - E^N_n\right)-i\eta} \tag{11}$$

$$= \sum_m \frac{\mathcal{X}^{\rm ph}_{\alpha\beta,m}\mathcal{X}^{\rm ph\dagger}_{\gamma\delta,m}}{E-\epsilon^{\rm ph+}_m+i\eta} - \sum_n \frac{\mathcal{Y}^{\rm ph\dagger}_{\alpha\beta,n}\mathcal{Y}^{\rm ph}_{\gamma\delta,n}}{E-\epsilon^{\rm ph-}_n-i\eta}. \tag{12}$$

The corresponding Bethe-Salpeter–type equation in the RPA reads as

$$\Pi^{\rm ph}_{\alpha\beta,\gamma\delta}(E) = \Pi^{\rm ph(0)}_{\alpha\beta,\gamma\delta}(E) + \sum_{\lambda,\mu}\Pi^{\rm ph(0)}_{\alpha\beta,\alpha\beta}(E)V_{\alpha\mu,\beta\lambda}\Pi^{\rm ph}_{\lambda\mu,\gamma\delta}(E) \tag{13}$$

$$= \Pi^{\rm ph(0)}_{\alpha\beta,\gamma\delta}(E) + \Pi^{\rm ph(0)}_{\alpha\beta,\alpha\beta}(E)\Gamma^{\rm ph}_{\alpha\beta,\gamma\delta}(E)\Pi^{\rm ph(0)}_{\gamma\delta,\gamma\delta}(E), \tag{14}$$

and defines the effective ph interaction $\Gamma^{\rm ph}$.

The actual calculation of the amplitudes and poles of the pp propagator and p-h polarization propagator can be done by solving the generalized eigenvalue problems [15]

$$\begin{pmatrix} A & B \\ B^\dagger & C \end{pmatrix}\begin{pmatrix} \mathcal{X}^{\rm pp+} & \mathcal{Y}^{\rm pp-} \\ \mathcal{Y}^{\rm pp+} & \mathcal{X}^{\rm pp-} \end{pmatrix} = \begin{pmatrix} \mathbb{1} & 0 \\ 0 & -\mathbb{1} \end{pmatrix}\begin{pmatrix} \mathcal{X}^{\rm pp+} & \mathcal{Y}^{\rm pp-} \\ \mathcal{Y}^{\rm pp+} & \mathcal{X}^{\rm pp-} \end{pmatrix}\begin{pmatrix} \epsilon^{\rm pp+} & 0 \\ 0 & \epsilon^{\rm pp-} \end{pmatrix}, \tag{15}$$

where

$$A_{\alpha\beta,\gamma\delta} = \tfrac{1}{2}(\delta_{\alpha\gamma}\delta_{\beta\delta} - \delta_{\alpha\delta}\delta_{\beta\gamma})(\epsilon_\alpha+\epsilon_\beta) + \tfrac{1}{2}V_{\alpha\beta,\gamma\delta}, \quad \alpha,\beta,\gamma,\delta > F \tag{16}$$

$$B_{\alpha\beta,\gamma\delta} = \tfrac{1}{2}V_{\alpha\beta,\gamma\delta}, \quad \alpha,\beta > F; \quad \gamma,\delta < F \tag{17}$$

$$C_{\alpha\beta,\gamma\delta} = \tfrac{1}{2}(\delta_{\alpha\gamma}\delta_{\beta\delta} - \delta_{\alpha\delta}\delta_{\beta\gamma})(\epsilon_\alpha+\epsilon_\beta) - \tfrac{1}{2}V_{\alpha\beta,\gamma\delta}, \quad \alpha,\beta,\gamma,\delta < F. \tag{18}$$

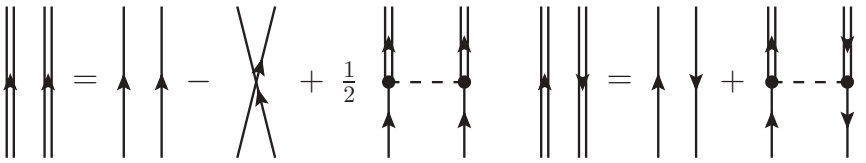

(a) (b)

FIG. 2. The diagrammatical representation of the (a) pp RPA equation and the (b) ph RPA equation where the single lines represent noninteracting, and the double lines interacting, propagators.

Here, the ϵ_α represent Hartree-Fock single-particle energies with the Fermi level F separating the occupied and unoccupied HF levels. The equations for the ph polarization propagator are again very similar:

$$\begin{pmatrix} D & E \\ E^* & D^* \end{pmatrix} \begin{pmatrix} \mathcal{X}^{\mathrm{ph}+} & \mathcal{Y}^{\mathrm{ph}-} \\ \mathcal{Y}^{\mathrm{ph}+} & \mathcal{X}^{\mathrm{ph}-} \end{pmatrix} = \begin{pmatrix} \mathbb{1} & 0 \\ 0 & -\mathbb{1} \end{pmatrix} \begin{pmatrix} \mathcal{X}^{\mathrm{ph}+} & \mathcal{Y}^{\mathrm{ph}-} \\ \mathcal{Y}^{\mathrm{ph}+} & \mathcal{X}^{\mathrm{ph}-} \end{pmatrix} \begin{pmatrix} \epsilon^{\mathrm{ph}+} & 0 \\ 0 & \epsilon^{\mathrm{ph}-} \end{pmatrix}, \tag{19}$$

where

$$D_{\alpha\beta,\gamma\delta} = \delta_{\alpha\gamma}\delta_{\beta\delta}(\epsilon_\alpha - \epsilon_\beta) + V_{\alpha\delta,\beta\gamma}, \quad \alpha,\gamma > F; \quad \beta,\delta < F \tag{20}$$

$$E_{\alpha\beta,\gamma\delta} = V_{\alpha\gamma,\beta\delta}, \quad \alpha,\gamma > F; \quad \beta,\delta < F. \tag{21}$$

C. Faddeev equations

The diagrammatic content of R can not be cast into the form of a Bethe-Salpeter equation without double counting of some classes of diagrams, in contrast to the more complicated four-times propagator (see Ref. [17]). This is why the Faddeev technique [18] must be used to split this object into three parts. The analysis will be done for $R^{2\mathrm{p1h}}$ (the derivation of $R^{2\mathrm{h1p}}$ is found to be completely analogous, but with an interchange of particle and hole lines). The decomposition of $R^{2\mathrm{p1h}}$ into three Faddeev components $R^{(i)}$ reads as

$$R^{2\mathrm{p1h}}_{\alpha\beta\gamma,\lambda\mu\nu}(E) = G^{(0)>}_{\alpha\beta\gamma,\lambda\mu\nu}(E) - G^{(0)>}_{\alpha\beta\gamma,\mu\lambda\nu}(E) + \sum_{i=1,2,3} R^{(i)}_{\alpha\beta\gamma,\lambda\mu\nu}(E), \tag{22}$$

where $G^{(0)>}$ is the part of the noninteracting 2p1h propagator with positive energy

$$G^{(0)>}_{\alpha\beta\gamma,\lambda\mu\nu}(E) = \frac{\delta_{\alpha\lambda}\delta_{\beta\mu}\delta_{\gamma\nu}}{E - (\epsilon_\alpha + \epsilon_\beta - \epsilon_\gamma) + i\eta}. \tag{23}$$

Together with its exchange counterpart, they form the free 2p1h propagator

$$R^{\mathrm{free}}_{\alpha\beta\gamma,\lambda\mu\nu}(E) = G^{(0)>}_{\alpha\beta\gamma,\lambda\mu\nu}(E) - G^{(0)>}_{\alpha\beta\gamma,\mu\lambda\nu}(E). \tag{24}$$

The relation between the different components $R^{(i)}$ can be derived from the diagrammatic content of Fig. 3. The superscripts (i), (j), and (k) are cyclical permutations of 1, 2, and 3 and correspond to the numbering of the fermion lines from left to right. In our notation, lines 1 and 2 are the particles and line 3 is the hole. Each propagator $R^{(i)}$ ends with lines j and k interacting through the adequate RPA interaction vertex, while all possible prior propagation is included in $R^{(j)}$, $R^{(k)}$, and the noninteracting propagators. $\Gamma^{(i)}$ is the extension to 2p1h space of Γ^{pp} and Γ^{ph} by adding a Kronecker delta for the third fermion line. The corresponding Bethe-Salpeter equations for the $R^{(i)}$,

$$R^{(i)}_{\alpha\beta\gamma,\lambda\mu\nu}(E) = \sum_{\zeta\eta,\theta} [G^{(0)>}\Gamma^{(i)}]_{\alpha\beta\gamma,\zeta\eta\theta}(E)\big[G^{(0)>}_{\zeta\eta\theta,\lambda\mu\nu}(E) - G^{(0)>}_{\zeta\eta\theta,\mu\lambda\nu}(E) + R^{(j)}_{\zeta\eta\theta,\lambda\mu\nu}(E) + R^{(k)}_{\zeta\eta\theta,\lambda\mu\nu}(E)\big], \tag{25}$$

form a closed self-consistent system.

The Lehmann representation

$$R^{(i)}_{\alpha\beta\gamma,\lambda\mu\nu} = \sum_m \frac{\mathcal{X}^{(i)}_{\alpha\beta\gamma,m}\mathcal{X}_{\lambda\mu\nu,m}}{E - \epsilon^{\mathrm{Fd}}_m + i\eta} - R^{(i)\mathrm{free}}_{\alpha\beta\gamma,\lambda\mu\nu} \tag{26}$$

follows from the Lehman representation for the full R (see Ref. [17]). The sum of the $R^{(i)\mathrm{free}}$ ensures that the noninteracting poles appearing in the first term of Eq. (22) are precisely canceled. The spectroscopic amplitude can be recovered by summing over the three Faddeev components

$$\mathcal{X}_{\alpha\beta\gamma,m} = \sum_{i=1,2,3} \mathcal{X}^{(i)}_{\alpha\beta\gamma,m}. \tag{27}$$

By multiplying Eq. (26) with $(E - \epsilon^{\mathrm{Fd}}_m)$ and taking the limit for $E \to \epsilon^{\mathrm{Fd}}_m$, the problem is reduced to a nonlinear eigenvalue problem for the spectroscopic amplitudes and the poles. The noninteracting poles do not coincide with the Faddeev poles, so the R^{free} is guaranteed to disappear when taking the limit

$$\mathcal{X}^{(i)}_{\alpha\beta\gamma,m} = \sum_{\zeta,\eta,\theta} (G^{(0)>}\Gamma^{(i)})_{\alpha\beta\gamma,\eta\zeta\theta}\big(\epsilon^{\mathrm{Fd}}_m\big)\big(\mathcal{X}^{(j)}_{\eta\zeta\theta,m} + \mathcal{X}^{(k)}_{\eta\zeta\theta,m}\big). \tag{28}$$

The explicit treatment of this equation for $i = 3$ (i.e., the pp channel) is given in Appendix A and is easily extended to the two other channels. When substituted in Eq. (28), we arrive at

$$\mathcal{X}^{(i)} = \left(U^{(i)}\frac{1}{\epsilon^{\mathrm{Fd}}_m - D^{(i)}}T^{(i)\dagger} + H^{(i)}H^{(i)\dagger}\right)(\mathcal{X}^{(j)} + \mathcal{X}^{(k)}). \tag{29}$$

The vectors $U^{(i)}$, $D^{(i)}$, $T^{(i)}$, and $H^{(i)}$ can be written in terms of the pp and ph amplitudes and energies. Their explicit form can be found in Appendix B. By introducing a vector containing these three components,

$$X = \begin{pmatrix} \mathcal{X}^{(1)} \\ \mathcal{X}^{(2)} \\ \mathcal{X}^{(3)} \end{pmatrix}, \tag{30}$$

this nonlinear equation in the Faddeev energies and amplitudes can be written in the form

$$X = \left(U\frac{1}{\epsilon^{\mathrm{Fd}} - D}T^\dagger + HH^\dagger\right)MX, \tag{31}$$

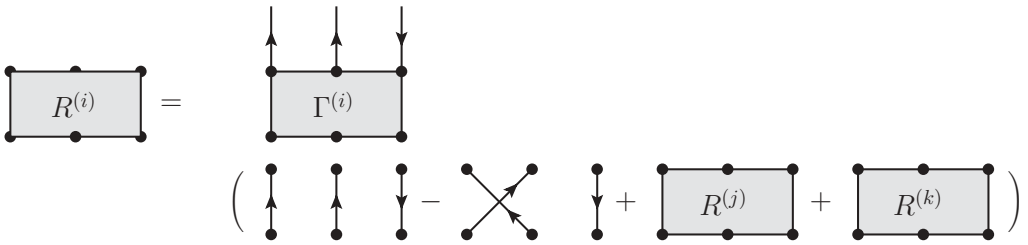

FIG. 3. Diagrammatic representation of Eq. (25).

where the matrix

$$M = \begin{pmatrix} 0 & \mathbb{1} & \mathbb{1} \\ \mathbb{1} & 0 & \mathbb{1} \\ \mathbb{1} & \mathbb{1} & 0 \end{pmatrix} \tag{32}$$

takes care of the coupling between the different channels. After some matrix algebra, this can be converted into a linear non-Hermitian eigenvalue problem

$$\epsilon^{\mathrm{Fd}} X = (\mathbb{1} - HH^{\dagger}M)^{-1} U[T^{\dagger}M + DU^{-1}(\mathbb{1} - HH^{\dagger}M)]X. \tag{33}$$

The matrix dimension of the eigenvalue problem is three times the size of the 2p1h basis. Two-thirds of the solutions are spurious and can be projected out, so the actual matrix dimension reduces to the size of a single 2p1h basis.

D. Handling spurious solutions

The use of Faddeev equations inherently introduces spurious solutions [24–26]. The solutions for which the sum in Eq. (27) is zero have no physical meaning and have to be discarded. At the same time, the vectors themselves will have to be antisymmetric under exchange of the first two particle or hole lines. By projecting the Hamiltonian matrix (33) onto the vector that has the right symmetry properties, and is nonvanishing when summed, the matrix dimension is reduced by a factor of 3. This vector space is spanned by the vector

$$\frac{1}{\sqrt{12}} \begin{pmatrix} \mathbb{1} - \mathbb{1}_{\mathrm{ex}} \\ \mathbb{1} - \mathbb{1}_{\mathrm{ex}} \\ \mathbb{1} - \mathbb{1}_{\mathrm{ex}} \end{pmatrix}, \tag{34}$$

where $(\mathbb{1}_{\mathrm{ex}})_{\alpha\beta\gamma,\lambda\mu\nu} = \delta_{\alpha\mu}\delta_{\beta\lambda}\delta_{\gamma\nu}$. The dimension of the matrix is now the same as in the standard ADC(3) matrix problem [13]. It can be verified that by using Tamm-Dancoff interactions and, after performing this projection, one regains the ADC(3) equations (see Appendix C).

E. Single-particle propagator and ground-state properties

The calculation of the FRPA single-particle propagator is now done by diagonalization of the symmetric matrix

$$F = \begin{array}{c} \\ p \text{ or } h \\ \text{2p1h} \\ \text{2h1p} \end{array} \begin{array}{c} \begin{array}{ccc} p \text{ or } h & \text{2p1h} & \text{2h1p} \end{array} \\ \begin{pmatrix} \epsilon & \tilde{U} & \tilde{U} \\ \tilde{U}^{\dagger} & \epsilon^{\mathrm{Fd}} & 0 \\ \tilde{U}^{\dagger} & 0 & \epsilon^{\mathrm{Fd}} \end{pmatrix} \end{array}, \tag{35}$$

where the ϵ^{Fd} matrices are diagonal and contain the 2p1h and 2h1p Faddeev energies. The tilde indicates that the coupling matrix elements are written in the basis that diagonalizes the Faddeev matrices

$$\tilde{U}_{\alpha,m} = \sum_{\lambda,\mu,\nu} U_{\alpha\nu,\lambda\mu} \mathcal{X}_{\lambda\mu\nu,m}. \tag{36}$$

Note that, in standard ADC(3), it is possible to write the equivalent of matrix (35) using (C6) and (6) as sub-blocks without a separate diagonalization in 2p1h and 2h1p space. This is not the case in the FRPA formalism as due to the non-Hermiticity of the right-hand side of Eq. (33). Thus, one should first diagonalize the 2p1h and 2h1p sub-blocks (that is, solve the Faddeev equations) and then write the matrix (35) in the new basis obtained. Performing the double diagonalization procedure therefore involves a doubling of the computer time with respect to the usual ADC(3) approach. In practical calculations, however, this is not the case since the dimension of matrix (35) can be reduced drastically by employing Arnoldi techniques in the 2p1h and 2h1p diagonalizations. This approach has been applied previously [20] and it was found that a limited number of Arnoldi vectors guarantee correct converged results for total energies and ionization potentials. In this paper, however, we did not resort to the Arnoldi algorithm and all results are obtained with full diagonalizations.

The diagonalization of (35) results in energies ω_n and residues $f_{\alpha,n}$ [see Eq. (2)], defining a new single-particle Green's function. By summing over the the solutions below the Fermi level, the density matrix

$$n_{\alpha,\beta} = \sum_{n<F} f_{\alpha,n} f^{*}_{\beta,n} \tag{37}$$

and the corresponding ground-state energy

$$E_0^N = \frac{1}{2}\left(\sum_{\alpha,\beta} \langle \alpha | T | \beta \rangle n_{\alpha\beta} + \sum_{\alpha} \sum_{n<F} \omega_n f_{\alpha,n} f^{*}_{\alpha,n} \right) \tag{38}$$

can be obtained, where T is the one-body part of the Hamiltonian.

In principle, full self-consistency could be achieved by iteratively recalculating the phonons on the basis of the new propagator and applying the Faddeev procedure. This, however, is computationally too demanding. We do improve the self-consistency of the solution by updating the Hartree-Fock–type static self-energy diagram. Instead of the diagonal matrix of single-particle energies, the Hartree-Fock self-energy calculated with the new density matrix elements $n_{\gamma,\delta}$

TABLE I. FRPA results for a set of small molecules in a cc-pVDZ basis set. The ground-state energy E_0 is given in hartree, the ionization energy I in electronvolt, equilibrium bond distances are in Angstrom, and the equilibrium angles in degrees. FRPA and FTDA refer to the calculations after the first iteration, while FRPA(c) and FTDA(c) refer to the calculations where consistency at the Hartree-Fock level was applied. The calculated data are compared to the coupled-cluster method at the level of CCSD(T) and to experimental data or exact calculations taken from Ref. [27]. The FCI energies were calculated at the FRPA(c) geometry.

Molecule		FTDA	FTDA(c)	FRPA	FRPA(c)	CCSD(T)	FCI	Expt.
H_2								
	E_0	−1.170	−1.161	−1.170	−1.161	−1.164	−1.164	−1.175
	r_{H-H}	0.769	0.757	0.770	0.757	0.761		0.741
	I	16.16	16.03	16.16	16.03	16.12		16.08
HF								
	E_0	−100.175	−100.224	−100.173	−100.228	−100.228	−100.231	
	r_{H-F}	0.904	0.916	0.897	0.913	0.920		0.917
	I	15.70	15.70	15.56	15.54	15.42		16.12
HCl								
	E_0	−460.295	−460.256	−460.293	−460.255	−460.254		
	r_{H-Cl}	1.314	1.297	1.314	1.293	1.290		1.275
	I	12.44	12.24	12.44	12.24	12.26		
BF								
	E_0	−124.331	−124.365	−124.332	−124.368	−124.380		
	r_{B-F}	1.285	1.284	1.305	1.285	1.295		1.267
	I	11.35	10.75	11.73	10.94	11.01		
BeH_2								
	E_0	−15.855	−15.831	−15.856	−15.832	−15.835	−15.836	
	r_{Be-H}	1.374	1.337	1.383	1.337	1.339		1.340
	I	11.89	11.78	11.84	11.76	11.89		
H_2O								
	E_0	−76.248	−76.240	−76.243	−76.236	−76.241		
	r_{H-O}	0.986	0.964	0.981	0.962	0.967		0.958
	Λ_{O-H-O}	101	102	100	102	102		104
	I	12.07	12.15	12.25	12.21	11.94		12.61
N_2								
	E_0		−109.258		−109.272	−109.276		
	r_{N-N}		1.104		1.106	1.119		1.098
	I		15.37		14.80	15.05		15.58
CO								
	E_0	−113.096	−113.037	−113.100	−113.048	−113.055		
	r_{C-O}	1.140	1.130	1.133	1.123	1.145		1.128
	I	14.39	13.69	14.23	14.44	13.64		14.01
CO_2								
	E_0		−188.139		−188.134	−188.148		
	r_{C-O}		1.162		1.162	1.175		1.162
	I		13.25		13.42	13.26		13.78
C_2H_2								
	E_0		−77.102		−77.093	−77.111		
	r_{C-C}		1.298		1.298	1.232		1.203
	r_{C-H}		1.083		1.080	1.081		1.063
	I		11.26		11.14	11.08		11.49

has to be included in the construction of the matrix F in Eq. (35):

$$\epsilon_{\alpha,\beta} = \langle\alpha|T|\beta\rangle + \sum_{\gamma,\delta}\langle\alpha\gamma|V|\beta\delta\rangle n_{\gamma,\delta}. \tag{39}$$

The implementation of this self-consistency will be indicated with a (c) attached to the method [FRPA(c), FTDA(c)]. Note that, both in FRPA and ADC(3), this partially self-consistent treatment is needed to include all static self-energy diagrams up to third order.

III. RESULTS AND DISCUSSION

The FRPA method is tested for a set of small molecules and its accuracy is evaluated by comparing to the ADC(3) method and to coupled-cluster calculations with single, double, and perturbative triple [CCSD(T)] excitations. The latter method should be of a comparable level of theory as both the ADC(3) and FRPA. Where possible, the comparison with full configuration interaction (FCI) and experimental results (or computational basis-set limits) [27–29] is also made.

TABLE II. Ionization energies in electronvolt calculated in the aug-cc-pVDZ basis set. The geometry was taken at the experimental value (See Table I). In the last two rows, the mean absolute deviation and maximum absolute deviation compared to experiment are given. The values between parentheses are calculated without the $1\sigma_u$ level of N_2. The column labeled ADC(3) represents the ADC(3) results from Ref. [28]. Experimental values are from Refs. [28,29].

HF	Level	HF	FTDA	FTDA(c)	ADC(3)	FRPA	FRPA(c)	Expt.
HF								
	1π	17.17	16.22	16.46	16.48	16.05	16.35	16.05
	3σ	20.98	20.14	20.33	20.36	20.03	20.24	20.0
CO								
	5σ	15.10	14.48	13.88	13.94	14.37	13.69	14.01
	1π	17.44	17.02	16.93	16.98	16.95	16.84	16.91
	4σ	21.99	20.05	20.11	20.19	19.46	19.59	19.72
N_2								
	$3\sigma_g$	17.25	16.14	15.65	15.72	15.76	15.18	15.60
	$1\pi_u$	16.73	17.20	16.82	16.85	17.71	17.14	16.98
	$2\sigma_u$	21.25	19.35	18.99	19.06	18.29	17.90	18.78
H_2O								
	$1b_1$	13.86	12.80	12.83	12.86	12.62	12.67	12.62
	$3a_1$	15.93	15.06	15.11	15.15	14.91	14.98	14.74
	$1b_2$	19.56	19.15	19.19	19.21	19.06	19.13	18.51
	$\bar{\Delta}$ (eV)	1.26(1.14)	0.34(0.31)	0.27(0.28)	0.30(0.30)	0.25(0.23)	0.31(0.26)	
	Δ_{max} (eV)	2.47(2.27)	0.64(0.64)	0.68(0.68)	0.70(0.70)	0.73(0.73)	0.88(0.62)	

A. Ground-state and ionization energies at equilibrium geometry

The FRPA fails to describe the correct dissociation behavior of diatomic molecules due to the appearance of instabilities in the RPA. The HF ground state becomes unstable with respect to ph excitations in the dissociation limit. The RPA Hamiltonian matrix is no longer positive-definite, which results in complex solutions to the RPA equations. All calculations were therefore performed at or close to the equilibrium geometry.

We first concentrate on calculating ground-state and ionization energies in equilibrium for a set of small molecules with a singlet ground state. For each method, calculations were performed for a number of different separation distances around the approximate equilibrium distance, after which a third-order polynomial was fitted to find the true energy minimum and equilibrium distance. For three molecules, we have also performed a FCI calculation. This was done at the FRPA(c) geometry, but within the quoted accuracy the same result holds for the CCSD(T) geometry. The results calculated in a correlation-consistent polarized valence double zeta (cc-pVDZ) basis set are presented in Table I.

The ground-state energies for the molecules H_2 to H_2O show little difference (at most 4 mH) between ADC(3) and FRPA. The differences for the other molecules, which have double or triple bonds, are somewhat larger, i.e., of the order of 10 mH. The FRPA(c) ground-state energies tend to be close to the CCSD(T) results with a maximum deviation of 18 mH in case of C_2H_2.

The equilibrium bond distances show a larger spread when comparing the Faddeev-Tamm-Dancoff approximation [FTDA(c)] and FRPA(c). The equilibrium bond distances for ADC(3) and FRPA have comparable deviations from the experimental values and, in the majority of cases, are closer to the experimental value than the CCSD(T) results. The FRPA(c) results are generally closer to the experimental value than ADC(3). The same conclusion can be made for the vertical ionization energies. The coupled-cluster results were calculated as the difference of the ground-state energies of the neutral and ionic molecule at the same geometry. The FTDA(c) and FRPA(c) ionization energies outperform the coupled-cluster results when the experimental value is available.

One remarkable fact is the lack of an equilibrium distance (no energy minimum) for N_2, CO_2, and C_2H_2 in both the FTDA and FRPA calculations without incorporating self-consistency at the level of the Hartree-Fock–type diagram. This example stresses the importance of a consistent treatment of the static self-energy. The inclusion of self-consistency in the calculations tends to adjust the results toward experiment, where needed.

To compare with previous ADC(3) calculations by other authors, we calculated ionization energies for a set of molecules with the settings used in Ref. [28], i.e., at the experimental geometries and with the augmented-cc-pVDZ (aug-cc-pVDZ) basis set. The results are presented in Table II. The present FTDA(c) results are in close agreement with the Dyson ADC(3) results in Ref. [28]. The differences are less than 2 mH and, in fact, are already present when comparing the Hartree-Fock single-particle energies. Compared to experiment, the mean absolute error is of the same order of magnitude for ADC(3) and FRPA. Note that there is a large deviation for the $2\sigma_u$ level of N_2 in the FRPA(c), which has a substantial influence on the mean error value.

We have also checked the basis-set dependency of the results by performing calculations for HF in the cc-pVDZ, correlation-consistent polarized valence triple zeta (cc-pVTZ), aug-cc-pVDZ, and augmented cc-pVTZ (aug-cc-pVTZ) basis sets. The differences in ionization energies between the basis sets with double zeta functions and these with triple zeta

TABLE III. Ground-state energies in hartree and vertical ionization energies in electronvolt for HF, calculated in different basis sets. The geometry was taken at the experimental value of 0.917 Å. Experimental values are from Refs. [28,29], and CCSD(T) and MP3 calculations were performed at the same geometry.

Method	Level	cc-pVDZ	aug-cc-pVDZ	cc-pVTZ	aug-cc-pVTZ	Expt.
FRPA						
	E_0	−100.172	−100.106	−100.335	−100.305	
	1π	15.46	16.05	16.19	16.33	16.11
	3σ	19.56	20.03	20.05	20.22	20.00
FRPA(c)						
	E_0	−100.228	−100.261	−100.346	−100.357	
	1π	15.54	15.35	16.16	16.41	16.11
	3σ	19.54	20.24	20.00	20.27	20.00
CCSD(T)						
	E_0	−100.228	−100.264	−100.338	−100.350	
	1π	15.44	16.06	15.96	16.16	16.11
MP3						
	E_0	−100.224	−100.256	−100.330	−100.340	
	1π	15.42	15.99	15.88	16.04	16.11

functions in Table III are of the order of 0.75 eV for the nonaugmented and 0.25 eV for the augmented basis sets. The convergence behavior of the ground-state energies calculated with FRPA(c) is very comparable to CCSD(T) and third order perturbation theory (MP3). The convergence in FRPA is weaker and again demonstrates the importance of self-consistency for the Hartree-Fock–type diagram. The correspondence between the MP3 ground-state energy and CCSD(T) is slightly worse in comparison to FRPA(c).

IV. CONCLUSION

In this paper, we have investigated the application of the FRPA technique to small molecules. The computational cost of this method is not much higher than that of the more established ADC(3) method and, in any case, lower than the cost for CCSD(T). The results at equilibrium geometry are comparable in accuracy to the ones obtained with the ADC(3) method, which is in line with the earlier atomic calculations in Ref [21]. The self-consistent treatment of the Hartree-Fock diagram has a positive effect on the numerical results and should always be included. While not superior to ADC(3) for small Coulomb systems, FRPA(c) has the promise of being a self-energy approximation that is applicable to both small and extended electronic systems.

However, a solution has to be found for the possible appearance of complex eigenvalues in the RPA and FRPA eigenvalue equations due to the inherent non-Hermiticity. A possible way out is to increase the self-consistency by allowing propagators with fragmented single-particle strength [19,30], which will be the object of future research.

ACKNOWLEDGMENTS

M.D. and D.V.N. are members of the Ghent-Brussels Quantum Chemistry and Molecular Modeling Alliance. M.D. acknowledges support by a grant provided by FWO-Flanders (Fund for Scientific Research). C.B. acknowledges the Japanese Ministry of Education, Science and Technology (MEXT) under KAKENHI Grant No. 21740213.

APPENDIX A: DERIVATION OF THE FRPA EQUATIONS FOR $i = 3$

The product of the forward-propagating uncorrelated 2p1h propagator and the interaction vertex is needed to find an expression in function of RPA amplitudes and the two-particle interaction. We will do this for the case $i = 3$; the other two cases are equivalent, but involve the $\Gamma^{\rm ph}$ instead of the $\Gamma^{\rm pp}$. The combination of the free 2p1h propagator and the vertex function can be written as

$$
\begin{aligned}
[G^{(0)>}\Gamma^{(3)}]_{\alpha\beta\gamma,\lambda\mu\nu}(E) &= \frac{1}{2}\int\frac{dE_1}{2\pi i}\int\frac{dE_2}{2\pi i}\sum_{\rho\sigma}G^{(0)>}_{\alpha,\rho}(E_2)G^{(0)>}_{\beta,\sigma}(E_1-E_2)G^{(0)<}_{\nu,\gamma}(E_1-E)\Gamma^{\rm pp}_{\rho\sigma,\lambda\mu}(E_1)\\
&= \frac{\delta_{\gamma\nu}}{2}\int\frac{dE_1}{2\pi i}\frac{1}{E_1-E-\epsilon_\gamma-i\eta}\Gamma^{\rm pp}_{\alpha\beta,\lambda\mu}(E_1)\int\frac{dE_2}{2\pi i}\frac{1}{E_2-\epsilon_\alpha+i\eta}\frac{1}{E_1-E_2-\epsilon_\beta+i\eta}\\
&= \frac{\delta_{\gamma\nu}}{2}\int\frac{dE_1}{2\pi i}\frac{1}{E_1-E-\epsilon_\gamma-i\eta}\Gamma^{\rm pp}_{\alpha\beta,\lambda\mu}(E_1)\frac{1}{E_1-\epsilon_\alpha-\epsilon_\beta+i\eta}. \qquad \text{(A1)}
\end{aligned}
$$

Here, the explicit expression for the phonon propagator is needed:

$$\begin{aligned}\Gamma^{\rm pp}_{\alpha\beta,\lambda\mu}(E) &= V_{\alpha\beta,\lambda\mu} + \frac{1}{4}\sum_{\rho,\sigma,\xi,\chi} V_{\alpha\beta,\rho\sigma} G^{\rm pp}_{\rho\sigma,\xi\chi}(E)\, V_{\xi\chi,\lambda\mu} \\ &= V_{\alpha\beta,\lambda\mu} + \frac{1}{4}\sum_{\rho,\sigma,\xi,\chi} V_{\alpha\beta,\rho\sigma}\left(\sum_m \frac{\mathcal{X}^{\rm pp}_{\rho\sigma,m}\mathcal{X}^{\rm pp\dagger}_{\xi\chi,m}}{E-\epsilon^{\rm pp+}_m+i\eta} - \sum_n \frac{\mathcal{Y}^{\rm pp}_{\xi\chi,n}\mathcal{Y}^{\rm pp\dagger}_{\rho\sigma,n}}{E-\epsilon^{\rm pp-}_n-i\eta}\right) V_{\xi\chi,\lambda\mu} \\ &= V_{\alpha\beta,\lambda\mu} + \sum_m \frac{\Delta^{\rm pp+}_{\alpha\beta,m}\Delta^{\rm pp+\dagger}_{\lambda\mu,m}}{E-\epsilon^{\rm pp+}_m+i\eta} - \sum_n \frac{\Delta^{\rm pp+}_{\lambda\mu,n}\Delta^{\rm pp+\dagger}_{\alpha\beta,n}}{E-\epsilon^{\rm pp-}_n-i\eta}. \end{aligned} \tag{A2}$$

The $\Delta^{\rm pp}$ are introduced as the product between the interaction and the normal RPA amplitudes $\mathcal{X}^{\rm pp}$ and $\mathcal{Y}^{\rm pp}$. Due to the RPA equations (15), this correspondence can also be expressed as

$$\mathcal{X}^{\rm pp}_{\alpha\beta,m} = \frac{\Delta^{\rm pp+}_{\alpha\beta,m}}{\left(\epsilon^{\rm pp+}_m - \epsilon_\alpha - \epsilon_\beta\right)}, \quad \mathcal{Y}^{\rm pp}_{\alpha\beta,n} = \frac{\Delta^{\rm pp-}_{\alpha\beta,n}}{\left(\epsilon^{\rm pp-}_n - \epsilon_\alpha - \epsilon_\beta\right)}. \tag{A3}$$

After performing the necessary integrations over the intermediate energies, one arrives at

$$\begin{aligned}[G^{(0)>}\Gamma^{(3)}]_{\alpha\beta\gamma,\lambda\mu\nu}(E) &= \frac{1}{2}\frac{\delta_{\gamma\nu}}{E-\epsilon_\alpha-\epsilon_\beta+\epsilon_\gamma+i\eta}\left(V_{\alpha\beta,\lambda\mu} + \sum_n \frac{\Delta^{\rm pp+}_{\alpha\beta,n}\Delta^{\rm pp+\dagger}_{\lambda\mu,n}}{E-\left(\epsilon^{\rm pp+}_n-\epsilon_\gamma\right)+i\eta}\right. \\ &\quad \left. + \sum_m \frac{\Delta^{\rm pp-}_{\alpha\beta,m}\Delta^{\rm pp-\dagger}_{\lambda\mu,m}\left(E-\epsilon_\alpha-\epsilon_\beta+\epsilon_\gamma-\epsilon_\lambda-\epsilon_\mu+\epsilon^{\rm pp-}_m\right)}{\left(\epsilon^{\rm pp-}_m-\epsilon_\alpha-\epsilon_\beta\right)\left(\epsilon^{pp-}_m-\epsilon_\lambda-\epsilon_\mu\right)}\right) \\ &= \frac{\delta_{\gamma\nu}}{2}\left(\sum_n \frac{\Delta^{\rm pp+}_{\alpha\beta,n}\Delta^{\rm pp+\dagger}_{\lambda\mu,n}}{\left(\epsilon^{\rm pp+}_n-\epsilon_\alpha-\epsilon_\beta\right)\left(E-\epsilon^{\rm pp+}_n+\epsilon_\gamma\right)} + \sum_m \frac{\Delta^{\rm pp-}_{\alpha\beta,m}\Delta^{pp-\dagger}_{\lambda\mu,m}}{\left(\epsilon^{\rm pp-}_m-\epsilon_\alpha-\epsilon_\beta\right)\left(\epsilon^{\rm pp-}_m-\epsilon_\lambda-\epsilon_\mu\right)}\right) \\ &= \frac{\delta_{\gamma\nu}}{2}\left(\sum_n \mathcal{X}^{\rm pp+}_{\alpha\beta,n}\frac{1}{E-\epsilon^{\rm pp+}_n+\epsilon_\gamma}\mathcal{X}^{\rm pp+\dagger}_{\lambda\mu,n}\left(\epsilon^{\rm pp+}_n-\epsilon_\lambda-\epsilon_\mu\right) + \sum_m \mathcal{Y}^{\rm pp-}_{\alpha\beta,m}\mathcal{Y}^{\rm pp-\dagger}_{\lambda\mu,m}\right), \end{aligned} \tag{A4}$$

here, in the second transition, the property $\Gamma^{\rm pp}_{\alpha\beta,\lambda\mu}(\epsilon_\alpha+\epsilon_\beta)=0$ was used to simplify the relation.

APPENDIX B: EXPLICIT FORM OF THE FRPA MATRICES

The matrices $U^{(i)}$, $T^{(i)}$, and $H^{(i)}$ are objects with left indices in the normal 2p1h space and right indices in the 2p1h space where the ith index is a single-particle state and the other two indices are combined either in a pp RPA or ph RPA phonon. For instance, for $U^{(3)}$ and $T^{(3)}$, the pp RPA phonon above the Fermi level with label n is combined into a 2p1h state with the hole state ν:

$$\begin{aligned} U^{(3)}_{\alpha\beta\gamma,n\nu} &= \frac{\delta_{\gamma\nu}}{\sqrt{2}}\mathcal{X}^{\rm pp+}_{\alpha\beta,n}, \\ T^{(3)}_{\alpha\beta\gamma,n\nu} &= \frac{\delta_{\gamma\nu}}{\sqrt{2}}\left(\epsilon^{\rm pp+}_n-\epsilon_\alpha-\epsilon_\beta\right)\mathcal{X}^{\rm pp+}_{\alpha\beta,n}, \end{aligned} \tag{B1}$$

while the pp RPA phonon under the Fermi level with label k is used for $H^{(3)}$:

$$H^{(3)}_{\alpha\beta\gamma,k\nu} = \frac{\delta_{\gamma\nu}}{\sqrt{2}}\mathcal{Y}^{\rm pp-}_{\alpha\beta,k}, \tag{B2}$$

where the factor $\frac{1}{\sqrt{2}}$ arises from the normalization condition for the pp RPA amplitudes and is not needed in case of ph RPA. The matrix $D^{(i)}$ is a diagonal matrix in the ith index and the phonon index:

$$D^{(3)}_{n\nu,n\nu} = \epsilon^{\rm pp+}_n - \epsilon_\nu. \tag{B3}$$

The use of the combined right index ensures the correct reproduction of Eq. (A4). The expressions for $i=1,2$ are analogous, except for the use of the ph phonons.

APPENDIX C: ADC(3) AS SPECIAL CASE OF FRPA

To show that ADC(3) is incorporated in FRPA, one has to change the RPA interactions with TDA interactions. This can be done by setting the off-diagonal blocks in Eqs. (15) and (19) to zero. As a result, there are no backward propagating amplitudes $\mathcal{Y}$. The FRPA equation (33) simplifies due to the disappearance of the $HH^\dagger$. After projecting out the spurious solutions, we get the equation >

$$\begin{aligned}\epsilon^{\rm Fd}\mathcal{X} = \frac{1}{12}(\mathbb{1}-\mathbb{1}_{\rm ex})\left(\sum_{i=1,2,3} U^{(i)}D^{(i)}U^{(i)-1} + 2U^{(i)}T^{(i)\dagger}\right) \\ \times(\mathbb{1}-\mathbb{1}_{\rm ex})\mathcal{X}. \end{aligned} \tag{C1}$$

As an example, we will again work out the term for $i = 3$ for the 2p1h energies

$$(U^{(3)}D^{(3)}U^{(3)-1} + 2U^{(3)}T^{(3)\dagger})_{\alpha\beta\gamma,\lambda\mu\nu} = \delta_{\gamma\nu}\sum_n \mathcal{X}^{\mathrm{pp}+}_{\alpha\beta,n}\left(\epsilon^{\mathrm{pp}+}_n - \epsilon_\nu\right)(\mathcal{X}^{\mathrm{pp}+})^{-1}_{\lambda\mu,n} + 2\delta_{\gamma\nu}\sum_n \mathcal{X}^{\mathrm{pp}+}_{\alpha\beta,n}\left(\epsilon^{\mathrm{pp}+}_n - \epsilon_\alpha - \epsilon_\beta\right)\mathcal{X}^{\mathrm{pp}+}_{\lambda\mu,n}. \quad \text{(C2)}$$

By eliminating the TDA eigenvalues and using their generating equations

$$\epsilon^{\mathrm{pp}+}_n \mathcal{X}^{\mathrm{pp}+}_{\alpha\beta,n} = (\epsilon_\alpha + \epsilon_\beta)\mathcal{X}^{\mathrm{pp}+}_{\alpha\beta,n} + \frac{1}{2}\sum_{\lambda,\mu} V_{\alpha\beta,\lambda\mu}\mathcal{X}^{\mathrm{pp}+}_{\lambda\mu,n} \quad \text{(C3)}$$

and using the orthonormality of the TDA eigenvectors

$$\sum_n \mathcal{X}^{\mathrm{pp}+}_{\alpha\beta,n}\mathcal{X}^{\mathrm{pp}+}_{\lambda\mu,n} = (\delta_{\alpha\lambda}\delta_{\beta\mu} - \delta_{\alpha\mu}\delta_{\beta\lambda}), \quad \text{(C4)}$$

we arrive at

$$(U^{(3)}D^{(3)}U^{(3)-1} + 2U^{(3)}T^{(3)\dagger})_{\alpha\beta\gamma,\lambda\mu\nu} = \delta_{\gamma\nu}[(\delta_{\alpha\lambda}\delta_{\beta\mu} - \delta_{\alpha\nu}\delta_{\beta\lambda})(\epsilon_\alpha + \epsilon_\beta - \epsilon_\gamma) + 3V_{\alpha\beta,\lambda\mu}]. \quad \text{(C5)}$$

Similar steps have to be taken for the other two channels. The sum of the three channels after antisymmetrization becomes

$$\left[\frac{1}{12}(\mathbb{1} - \mathbb{1}_{\mathrm{ex}})\left(\sum_{i=1,2,3} U^{(i)}D^{(i)}U^{(i)-1} + 2U^{(i)}T^{(i)\dagger}\right)(\mathbb{1} - \mathbb{1}_{\mathrm{ex}})\right]_{\alpha\beta\gamma,\lambda\mu\nu} = \delta_{\gamma\nu}(\delta_{\alpha\lambda}\delta_{\beta\mu} - \delta_{\alpha\mu}\delta_{\beta\lambda})(\epsilon_\alpha + \epsilon_\beta - \epsilon_\gamma) + \delta_{\gamma\nu}V_{\alpha\beta,\lambda\mu} + \delta_{\alpha\lambda}V_{\beta\nu,\mu\gamma} + \delta_{\beta\mu}V_{\alpha\nu,\lambda\gamma} - \delta_{\alpha\mu}V_{\beta\nu,\lambda\gamma} - \delta_{\beta\lambda}V_{\alpha\nu,\mu\gamma}. \quad \text{(C6)}$$

This is exactly the same expression as in ADC(3). The FTDA and ADC(3) are completely equivalent.

[1] S. R. White, Phys. Rev. Lett. **69**, 2863 (1992).
[2] G. K.-L. Chan, J. J. Dorando, D. Ghosh, J. Hachmann, E. Neuscamman, H. Wang, and T. Yanai, in *Frontiers in Quantum Systems in Chemistry and Physics*, Progress in Theoretical Chemistry and Physics, Vol. 18, edited by J. Maruani *et al.* (Springer, Netherlands, 2008), pp. 49–65.
[3] R. J. Bartlett, Annu. Rev. Phys. Chem. **32**, 359 (1981).
[4] D. M. Ceperley and L. Mitas, in *New Methods in Computational Quantum Mechanics*, edited by I. Prigogine and S. Rice (Wiley, New York, 1996).
[5] P. H. Acioli, J. Mol. Struct. **394**, 75 (1997).
[6] D. Pines, *The Many-Body Problem* (Benjamin, Reading, MA, 1962).
[7] A. L. Fetter and J. D. Walecka, *Quantum Theory of Many-Particle Systems* (McGraw-Hill, San Francisco, 1971).
[8] W. H. Dickhoff and D. Van Neck, *Many Body Theory Exposed!*, 2nd ed. (World Scientific, Singapore, 2008).
[9] J. Linderberg and Y. Öhrn, *Propagators in Quantum Chemistry* (Academic, London, 1973).
[10] L. S. Cederbaum and W. Domcke, Adv. Chem. Phys. **36**, 205 (1977).
[11] W. von Niessen, J. Schirmer, and L. S. Cederbaum, Comput. Phys. Rep. **1**, 57 (1984).
[12] J. V. Ortiz, in *Computational Chemistry: Reviews of Current Trends*, edited by J. Leszcynski, Vol. 2 (World Scientific, Singapore, 1997), Chap. 1.
[13] J. Schirmer, L. S. Cederbaum, and O. Walter, Phys. Rev. A **28**, 1237 (1983).
[14] M. S. Deleuze, M. G. Giuffreda, J.-P. François, and L. S. Cederbaum, J. Chem. Phys. **111**, 5851 (1999).
[15] P. Ring and P. Schuck, *The Nuclear Many-Body Problem* (Springer, New York, 1980).
[16] G. A. Rijsdijk, W. J. W. Geurts, K. Allaart, and W. H. Dickhoff, Phys. Rev. C **53**, 201 (1996).
[17] C. Barbieri and W. H. Dickhoff, Phys. Rev. C **63**, 034313 (2001).
[18] L. D. Faddeev, *Mathematical Aspects of the Three-Body Problem in the Quantum Scattering Theory* (Israel Program for Scientific Translations, Jerusalem, Israel, 1965).
[19] C. Barbieri and W. H. Dickhoff, Phys. Rev. C **65**, 064313 (2002).
[20] C. Barbieri and M. Hjorth-Jensen, Phys. Rev. C **79**, 064313 (2009).
[21] C. Barbieri, D. Van Neck, and W. H. Dickhoff, Phys. Rev. A **76**, 052503 (2007).
[22] S. Ethofer and P. Schuck, Z. Phys. A **228**, 264 (1969).
[23] J. Winter, Nucl. Phys. **194**, 535 (1972).
[24] S. K. Adhikari and W. Glöckle, Phys. Rev. C **19**, 616 (1979).
[25] J. W. Evans and D. K. Hoffman, J. Math. Phys. **22**, 2858 (1981).
[26] P. Navrátil, B. R. Barrett, and W. Glöckle, Phys. Rev. C **59**, 611 (1999).
[27] NIST Computational Chemistry Comparison and Benchmark Database, *NIST Standard Reference Database Number 101 Release 15a* (2010).
[28] A. B. Trofimov and J. Schirmer, J. Chem. Phys. **123**, 144115 (2005).
[29] K. Kimura, S. Katsumata, Y. Achiba, T. Yamazaki, and S. Iwata, *Handbook of HeI Photoelectron Spectra of Fundamental Organic Molecules* (Halsted, New York, 1981).
[30] C. Barbieri and W. H. Dickhoff, Phys. Rev. C **68**, 014311 (2003).